First publ. in: Journal of Biological Chemistry 280 (2005), 30, pp. 27960-27969

Quantitative Calcium Measurements in Subcellular Compartments of *Plasmodium falciparum*-infected Erythrocytes*

Petra Rohrbach‡§, Oliver Friedrich‡§¶, Joachim Hentschel‖, Helmut Plattner‖, Rainer H. A. Fink¶, and Michael Lanzer‡**

From the ‡Hygiene Institut, Abteilung Parasitologie, Universitätsklinikum Heidelberg, Im Neuenheimer Feld 324, D-69120 Heidelberg, the ¶Medical Biophysics, Institute of Physiology and Pathophysiology, University of Heidelberg, Im Neuenheimer Feld 326, D-69120 Heidelberg, and the ‖Department of Biology, University of Konstanz, D-78457 Konstanz, Germany

The acidic food vacuole exerts several important functions during intraerythrocytic development of the human malarial parasite *Plasmodium falciparum*. Hemoglobin taken up from the host erythrocyte is degraded in the food vacuole, and the heme liberated during this process is crystallized to inert hemozoin. Several antimalarial drugs target food vacuolar pathways, such as hemoglobin degradation and heme crystallization. Resistance and sensitization to some antimalarials is associated with mutations in food vacuolar membrane proteins. Other studies suggest a role of the food vacuole in ion homeostasis, and release of Ca^{2+} from the food vacuole may mediate adopted physiological responses. To investigate whether the food vacuole is an intracellular Ca^{2+} store, which in turn may affect other physiological functions in which this organelle partakes, we have investigated total and exchangeable Ca^{2+} within the parasite's food vacuole using x-ray microanalysis and quantitative confocal live cell Ca^{2+} imaging. Apparent free Ca^{2+} concentrations of ~90, ~350, and ~400 nM were found in the host erythrocyte cytosol, the parasite cytoplasm, and the food vacuole, respectively. In our efforts to determine free intracellular Ca^{2+} concentrations, we evaluated several Ca^{2+}-sensitive fluorochromes in a live cell confocal setting. We found that the ratiometric Ca^{2+} indicator Fura-Red provides reliable determinations, whereas measurements using the frequently used Fluo-4 are compromised due to problems arising from phototoxicity, photobleaching, and the strong pH dependence of the dye. Our data suggest that the food vacuole contains only moderate amounts of Ca^{2+}, disfavoring a role as a major intracellular Ca^{2+} store.

Malaria is one of the major causes of morbidity and mortality in developing countries. Of the four parasites that can cause malaria in humans, *Plasmodium falciparum* is the most virulent, being responsible for an estimated 300–500 million clinical cases and 1–3 million deaths, mainly children, annually (1).

P. falciparum is an obligatory intracellular parasite that propagates within human hepatocytes and erythrocytes. During intraerythrocytic development, malaria parasites tightly regulate their intracellular Ca^{2+} concentration, and sudden increases in cytosolic Ca^{2+} can trigger cell signaling events and developmental processes (2). Growth of the parasite can be inhibited by a range of Ca^{2+} ionophores, Ca^{2+} channel blockers, and Ca^{2+}/calmodulin antagonists (reviewed in Ref. 3), suggesting that factors maintaining Ca^{2+} homeostasis are valid targets for drug intervention. Although several Ca^{2+} carriers, including Ca^{2+}-ATPases, have been identified and characterized (4–6), the total and free subcellular Ca^{2+} distribution, as well as the mechanisms of intracellular Ca^{2+} homeostasis, are still not well understood in the parasite, and the methods used for steady-state and dynamic Ca^{2+} measurements are continuously being modified.

P. falciparum induces dramatic changes in the global $[Ca^{2+}]_i$ of its host erythrocyte (7). Typically, the free $[Ca^{2+}]_i$ in human erythrocytes does not exceed the lower nM range (~50–150 nM) (8, 9). However, a continuous net uptake of Ca^{2+} occurs as the parasite matures (10), which has been attributed to an increased Ca^{2+} permeability of the host erythrocyte plasma membrane (11, 12). The parasite's cytoplasm is thought to contain a low free $[Ca^{2+}]_i$ of ~100 nM (13), similar to that of other eukaryotic cells (14), although quantitative determinations are controversial, ranging from 50 to 700 nM (15, 16). Early during intraerythrocytic development, high concentrations of Ca^{2+} appear to accumulate transiently in the parasitophorous vacuole (17), which separates the parasite from the erythrocyte cytosol. Other subcellular organelles considered to serve as intracellular Ca^{2+} stores are the parasite's endoplasmic reticulum (ER),[1] the food vacuole (16, 18), and the acidocalcisomes (15, 18–22).

As shown for the related apicomplexan parasite *Toxoplasma gondii*, as well as for trypanosomatids, acidocalcisomes are electron-dense organelles containing high levels of calcium, phosphorus, magnesium, and other elements (22–24), with most of the Ca^{2+} up to molar levels bound to polyphosphates (22, 25). A recent study has presented evidence for the presence of a calcium- and phosphorus-rich, electron-dense organelle in the merozoite (26), the invasive stage of the parasite.

The food vacuole is an acidic organelle in which the erythrocyte hemoglobin is digested (27, 28) and the toxic byproduct heme is crystallized to inert hemozoin (28). It is the site of action of several antimalarial drugs (29), and within its membrane, it contains transporters implicated in drug resistance mechanisms (30).

A possible function of the food vacuole in Ca^{2+} storage was

* This work was supported by the Landesstiftung Baden-Württemberg. The costs of publication of this article were defrayed in part by the payment of page charges. This article must therefore be hereby marked "*advertisement*" in accordance with 18 U.S.C. Section 1734 solely to indicate this fact.

§ Both authors contributed equally to this study.

** To whom correspondence should be addressed. Tel.: 49-6221-567845; Fax: 49-6221-564643; E-mail: michael_lanzer@med.uni-heidelberg.de.

[1] The abbreviations used are: ER, endoplasmic reticulum; CPA, cyclopiazonic acid; TG, thapsigargin.

deduced from live cell confocal laser scanning microscopy using Fluo-4 as a Ca^{2+} indicator (16). The intense Fluo-4 fluorescence observed from the acidic food vacuole, as compared with the parasite's cytoplasm, was interpreted in terms of a model in which the food vacuole serves as a dynamic intracellular Ca^{2+} store (16), similar to the situation in plants in which the tonoplast can store millimolar concentrations of Ca^{2+} (31), mainly complexed with phosphorus (32).

However, the interpretation of Fluo-4 signals is complicated by the following. (i) Fluo-4 does not allow for ratiometric measurements, *i.e.* the signal depends on dye loading and/or partitioning and cannot be readily referred to Ca^{2+} concentrations. (ii) Fluo-4 fluorescence is potentially pH-dependent, as has been shown for the related fluorochrome fluorescein (33). If Fluo-4 fluorescence also exhibits a pH dependence, then this must be taken into account when Fluo-4 fluorescence signals are compared between subcellular compartments of vastly different pH values such as the parasite's cytoplasm (pH ~7.3) and the acidic food vacuole (pH ~5.4) (30). (iii) The food vacuole of *P. falciparum* is light-sensitive (34). Photo damage to its membrane and subsequent lysis quickly arise during microscopy due to photo-induced lipid peroxidation (34). Whether Fluo-4 can also sensitize photo-damaging reactions is not yet investigated.

As the food vacuole is an important organelle in the physiology of the parasite, we have reinvestigated steady-state and dynamic free $[Ca^{2+}]_i$ in this compartment using, in a confocal setting, Ca^{2+}-sensitive fluorochromes including Fluo-4, Fura-2, and Fura-Red. In addition, using x-ray microanalysis, we have examined the total calcium, phosphorus, and iron content of the food vacuole. Our data are interpreted in terms of a model suggesting that the parasite's food vacuole does not act as a major internal Ca^{2+} store.

EXPERIMENTAL PROCEDURES

Chemicals—Fura-2 acetoxymethylester (AM), Fura-Red-AM, Fluo-4-AM, LysoSensor Blue DND-192, ER-Tracker Blue-White DPX, and Pluronic F-127 were purchased from Molecular Probes (Leiden, Netherlands). Inhibitors of the sarco/endoplasmic reticulum calcium ATPase thapsigargin (TG) and cyclopiazonic acid (CPA) were obtained from Calbiochem. The H^+ ionophore nigericin was purchased from Sigma, and the Ca^{2+} ionophore ionomycin was purchased from Calbiochem.

P. falciparum Culture—*P. falciparum* parasites were maintained in continuous *in vitro* cultures as described previously (35). Live cell experiments were carried out using the *P. falciparum* clones Dd2 and K1. Trophozoite stage parasites were used in all experiments.

Dye Loading of P. falciparum Parasites—*P. falciparum*-infected erythrocytes were washed twice with Ringer's solution (122.5 mM NaCl, 5.4 mM KCl, 1.2 mM $CaCl_2$, 0.8 mM $MgCl_2$, 11 mM D-glucose, 10 mM HEPES, 1 mM NaH_2PO_4, pH 7.4) and loaded with 5 μM Fluo-4-AM, 5 μM Fura-2-AM, 9 μM Fura-Red-AM, or 500 nM ER-Tracker Blue-White DPX in Ringer's solution with Pluronic F-127 (0.1% v/v) for 45 min to 1 h at 37 °C. Dye-loaded parasites were settled onto poly-L-lysine-coated coverslips in a microperfusion chamber as described previously (36, 37). Unbound parasites and remaining dye were washed away by perfusion with Ringer's solution. For the double labeling experiments, Ringer's solution was supplemented with the fluorescent dye LysoSensor Blue DND-192 at a concentration of 1 μM.

Live Cell Imaging—Confocal laser scanning fluorescence microscopy was performed using a Zeiss LSM510 (Carl Zeiss, Jena, Germany) equipped with UV and visible laser lines (351, 364, 458, and 488 nm) and an Axiovert 100M microscope. For Fluo-4-AM and LysoSensor Blue DND-192 double-labeling, the laser lines and filter settings used in Multi-Track mode were as follows: LysoSensor Blue DND-192 excited at 364 nm with emission detected using the LP 385-nm filter (blue channel), and Fluo-4-AM excited at 488 nm with emission using LP 505-nm filter (green channel). For optimization, the following settings were used: excitation at 488 nm with 1% transmission (argon laser, 25 milliwatt), and excitation at 364 nm with 2% transmission (UV laser, 80 milliwatt). Single images were obtained using a ×63 lens (C-APO, N.A. = 1.2) with an 8-fold software zoom, 512 × 512 pixel. For ratiometric Ca^{2+} imaging using Fura-2-AM, dual excitation ratio images of Fura-2-AM were acquired using 351 and 364-nm UV laser lines and a 505-nm-long pass emission filter. The line-wise Multi-Track mode was used to collect image fluorescence. Images were collected every 5 s. To record the excitation spectra of Fura-2 stained parasites, Fura-2 was excited with a polychromator (PolyChrom III, Till-Photonics) in 1-nm steps between 280 and 500 nm, and fluorescence was collected with a fixed filter setting in the visible light range (>510 nm) in an epifluorescence setup (Visitron Imaging Systems). For ratiometric confocal Fura-Red Ca^{2+} imaging, Fura-Red was alternately excited with the 458- and 488-nm argon laser lines. The transmittance for the 458-nm line was 9 and 1% for the 488-nm line. Fura-Red fluorescence was measured using a 570-nm-long pass filter, resulting in a pair of images ($F_{458\ nm}$ and $F_{488\ nm}$). The Ca^{2+} inhibitors TG (1 μM) and CPA (10 μM) were added to a time series in the absence and presence of 10 μM nigericin. Note: Fura-Red is a calcium-quenching fluorophore, *i.e.* an increase in fluorescence corresponds to a decrease in Ca^{2+} concentration for both excitation wavelengths. However, the ratio $F_{458\ nm}/F_{488\ nm}$ increases with rising Ca^{2+} concentration (38). For ER-Tracker Blue-White DPX imaging, the dye was excited at 364 nm with emission detected using a LP385 emission filter. For all confocal laser scanning fluorescence microscopy, a pinhole of 1.2 μm (1.34 Airy units) was chosen to ensure that fluorescence was from within the food vacuole and not regions lying above or below. *P. falciparum* Dd2 trophozoites were used unless stated otherwise.

Fluorochrome pH Dependence—In situ experiments were performed as follows. Parasites were loaded with 5 μM Fluo-4-AM or 9 μM Fura-Red-AM at 37 °C for 45 min and then added to a chamber as described above. A time course was started, and measurements were taken every 5 s. Ringer's solution was prepared with varying pH (5.5, 6.5, 7.5) and supplied with 10 μM nigericin. This buffer was applied to the time course measurement, and the change in fluorescence was quantified. For *in vitro* experiments, 5 μM Fluo-4-AM or 9 μM Fura-Red-AM was added to Ringer's solution containing a fixed free Ca^{2+} concentration of 350 nM. pH values were adjusted ranging from 5.0 to 8.0. Using an Aminco Bowman Series 2 luminescence spectrometer, emission scans were performed for each pH with a step size of 1 nm ranging from 500 to 600 nm for Fluo-4 and from 520 to 700 nm for Fura-Red. For Fluo-4, the spectra were integrated starting from 505 nm (LP 505 nm) and starting from 570 nm (LP 570 nm) for Fura-Red to ensure identical conditions for the fluorescence evaluation as in the confocal *in situ* setting.

Data Analysis—P. falciparum-infected erythrocytes were readily identified by eye. Using the LSM510 v3.2 software, a region of interest, including either the vacuole or the cytosol of the parasite, was defined. The mean ratio value of the region of interest was measured throughout the image sequence. The measured fluorescence was further analyzed using Excel (Microsoft), Sigma Plot (SPSS software), Origin (Microcal Systems), and ImageJ (NIH software). Images were processed using Corel Draw and Corel Photopaint.

In Situ Ca^{2+} Calibration of Fura-Red—A confocal laser scanning microscope (Carl Zeiss) and the fluorescent calcium indicator Fura-Red-AM was used to measure the intracellular free calcium concentration. The mean vacuolar and cytoplasmic ratios ($R_{458/488}$) were evaluated in the intact parasite (*i.e.* resting $[Ca^{2+}]_i$) as well as after permeabilizing the membranes using the Ca^{2+} ionophore ionomycin (10 μM) and clamping the external solution to various free Ca^{2+} values as described in Ref. 39. R_{min} corresponds to ratios in Ca^{2+}-free solution (~1 nM), and R_{max} corresponds to ratios in the presence of saturating free Ca^{2+} (~1 mM, see Ref. 39). A calibration curve was fitted to this Ca^{2+}-$R_{458/488}$ relationship using a least square fit to a Hill function. The Hill coefficient was fixed to unity reflecting the 1:1 stoichiometry of Fura-Red binding to Ca^{2+} ions. In some analyses, the Hill coefficient was set as a free variable and accurately predicted a value close to unity (not shown). The $R_{458/488}$ were then converted to corresponding resting free $[Ca^{2+}]_i$ values using the inverse Hill equation, and a Grubbs test was performed to identify outliers (at the $p = 0.05$ level). Outliers of the resting $R_{458/488}$ were omitted from further analysis. Finally, mean resting free $[Ca^{2+}]_i$ from the vacuole and the cytoplasmic area were compared using a Student's t test at the $p = 0.05$ level.

X-ray Microanalysis—X-ray microanalysis was performed on either whole cells, air-dried onto Formvar-coated grids, or cryofixed, sectioned cells. For cryofixation, infected erythrocytes were spray-frozen into liquid propane (×180 °C) using the quenched flow method (40). After removing the propane under vacuum at ×100 °C in a GT1 freeze dryer (Leybold Heraeus), cells were freeze-substituted for 48 h at ×80 °C in dry methanol containing 3% glutaraldehyde, 1% OsO_4, and 250 mM KF to retain free calcium, based on previous work (41, 42). After freeze substitution, the temperature was slowly raised to +4 °C (overnight),

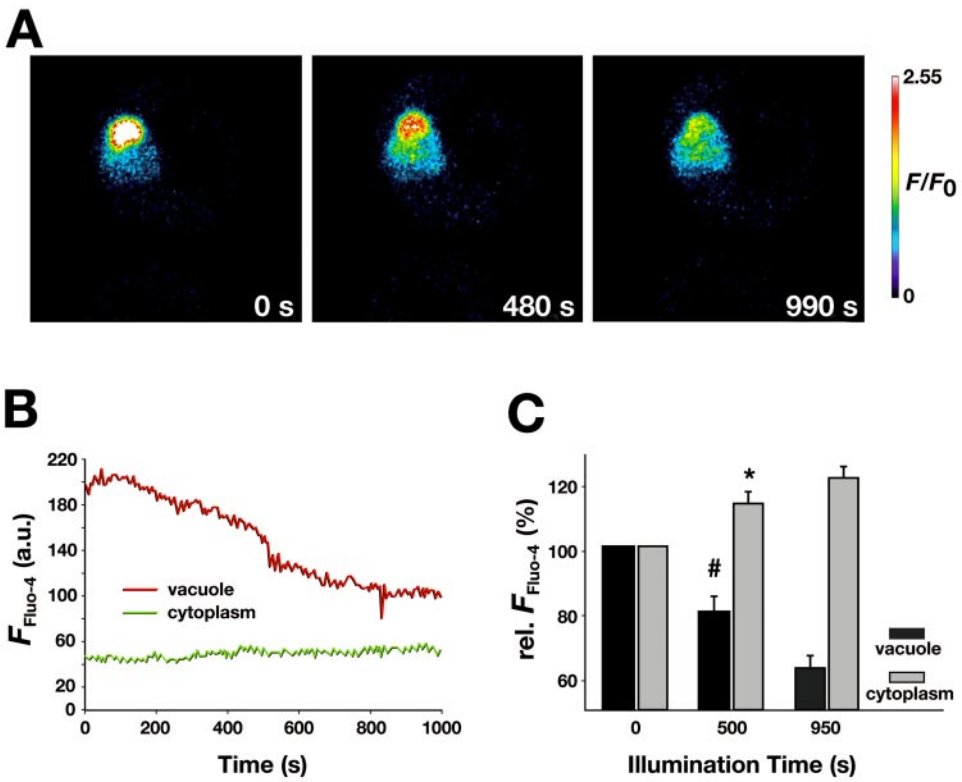

FIG. 1. **Dynamic changes in live cell Fluo-4 imaging of *P. falciparum*-infected erythrocytes.** *A*, three images of a representative time series using recurrent illumination in a Fluo-4 stained *P. falciparum*-infected erythrocyte at 0, 480, and 990 s. During the Fluo-4 imaging, the fluorescence intensity dramatically drops in the vacuolar compartment (see the *pseudocolor scale*; 2.55 = high fluorescence intensity, 0 = no fluorescence intensity). *Scale bar*, 4 μm. *B*, the time course of Fluo-4 fluorescence intensity in the regions of interest depicting the food vacuole (*red line*) and the parasite cytoplasm (*green line*) of the parasite shown in *A*. *C*, Fluo-4 Ca^{2+} fluorescence intensities evaluated at the times shown in *A* for the vacuole and cytoplasm of 10 parasites normalized to their initial values at 0 s (100%). Relative fluorescence is already significantly reduced in the food vacuole (#, $p < 0.05$) after 480 s and increases in the cytoplasm (*, $p < 0.01$), indicating vacuolar damage. *a.u.*, arbitrary units.

and cells were finally embedded in Spurr's resin. Analysis was performed on 500-nm-thick sections. X-ray microanalysis of cryofixed sections has been successfully and reliably used to localize total Ca^{2+} in specific subcellular compartments (41–44). Specimens were analyzed using a 912 Omega scanning transmission electron microscope (Carl Zeiss). X-rays were collected using a lithium-drifted silicon detector (front area 30 mm^2) equipped with an ATW atmospheric window. The microscope was operated as follows: 80 kV tungsten filament, scanning transmission, and imaging mode (scanning transmission electron micrographs); spot size was 63 nm, and emission current was ~10 μA, according to Ref. 43. Analysis was performed using the INCA EDX microanalysis software (Oxford Instruments).

RESULTS

Temporal Changes in Fluo-4 Imaging—Staining of *P. falciparum*-infected erythrocytes with the Ca^{2+} fluorophore Fluo-4 was analyzed using a confocal laser scanning microscope and experimental settings as described previously (16). In accordance with the published data, we observed a strong Fluo-4 fluorescence signal originating from the parasite's acidic food vacuole, a weak signal from the parasite cytoplasm, and hardly any from the erythrocyte cytoplasm (Fig. 1*A*). However, the food vacuolar fluorescence signal was unstable and declined with recurrent illumination (Fig. 1, *B* and *C*). The drop in Fluo-4 fluorescence intensity in the vacuole coincided with an increase in cytoplasmic fluorescence (Fig. 1, *B* and *C*).

We repeated Fluo-4 imaging in the presence of LysoSensor Blue DND-192 (LS Blue), an acidotropic probe that accumulates in the parasite's food vacuolar compartment (34). Initially, both Fluo-4 and LS Blue fluorescence signals co-localized in the food vacuole (Fig. 2*A*). However, within one to 2 min, both Fluo-4 and LS Blue fluorescence faded from the food vacuole and were redistributed to the parasite's cytoplasm (Fig. 2*B*). These data indicated that Fluo-4 fluorescence signals are unstable and change over time. Possible explanations for this effect are provided under "Discussion."

Fluo-4 Fluorescence Is pH-dependent—Given that the pH in the parasite's cytoplasm and acid food vacuole differs by approximately two pH units, we considered the influence of pH on the Fluo-4 fluorescence signal. To this end, the pH of the *P. falciparum*-infected erythrocytes loaded with Fluo-4 was clamped to values ranging from 7.5 to 5.5. pH-induced changes in fluorescence intensity (ΔF) were determined, normalized to the value obtained in Ringer's solution at a pH of 7.3 (F_0), and analyzed as a function of the pH. A substantial pH dependence of the Fluo-4 fluorescence signal was observed *in situ* (Fig. 3*A*). To clarify whether this finding represents a direct effect of the dye or is due to indirect influences of the food vacuolar environment on the fluorescence signal, the pH dependence was determined *in vitro* using a fluorospectrometer for the Fluo-4 fluorochrome alone. Again, a strong pH dependence was observed, with the fluorescence increasing as the pH decreases (Fig. 3*B*). A maximum was reached at pH 6.25, after which the fluorescence declined (Fig. 3*C*).

Evaluation of Ratiometric Fluorescent Ca^{2+} Indicators—The data presented above suggest that Fluo-4 fluorescence is strongly pH-dependent, thus complicating the interpretation of data obtained from cellular compartments varying in pH. We therefore searched for ratiometric fluorescent Ca^{2+} indicators with chemical structures different from Fluo-4 and pH independence. We initially tested the UV light-excitable Fura-2 fluorophore, a widely used ratiometric Ca^{2+} indicator with a reported isosbestic point of ~360 nm (for a review on Ca^{2+} indicators, see Ref. 45). *P. falciparum*-infected erythrocytes loaded with Fura-2 revealed a strong and stable fluorescence signal from both the cytoplasm and the food vacuole when

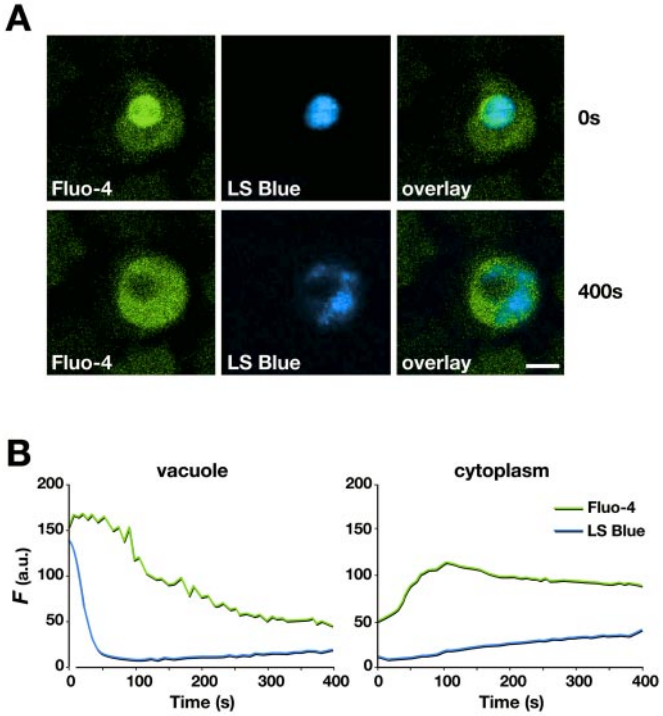

FIG. 2. **Photolysis of the food vacuolar membrane confirmed by confocal imaging with LysoSensor Blue DND-192.** *A*, images from a representative parasite double-stained with Fluo-4 (*left*) and LS Blue (*middle*) at 0 (*top*) and 400 s (*bottom*) after recurrent illumination (*right*, overlay images of fluorescence signals). *Scale bar*, 2.5 μm. *B*, time course of Fluo-4 (*green line*) and LS Blue (*blue line*) fluorescence intensity in the food vacuole (*left*) and the cytoplasm (*right*) of the same parasite. LS Blue fluorescence markedly drops within the first 50 s and redistributes into the cytoplasm. The same observation can be made for Fluo-4 fluorescence although occurring with a slower kinetics. *a.u.*, arbitrary units.

excited with 351- and 364-nm UV laser lines (Fig. 4*A*). To monitor dynamic Ca^{2+} changes, we increased the laser power such that the food vacuolar membrane would lyse and monitored the time course of fluorescence intensities $F_{351\ nm}$ and $F_{364\ nm}$. As expected, the fluorescence measured from the food vacuole rapidly decreased, whereas that from the parasite cytoplasm slightly increased with time (Fig. 4*B*). However, the kinetics of $F_{351\ nm}$ and $F_{364\ nm}$ was very similar for both vacuolar and cytoplasmic recordings (Fig. 4*B*). This was inconsistent with a ratiometric measurement. Moreover, the ratios of $F_{351\ nm}$ over $F_{364\ nm}$ remained constant with time (Fig. 4*B*). These findings suggested that the isosbestic point has shifted in our specimen, a phenomenon that has also been described in other cell types (45). Indeed, recording the excitation spectra in the parasites, in an epifluorescence setting with a polychromator, revealed a strong red shift in the Ca^{2+}-dependent Fura-2 spectra with the isosbestic point being close to 380 nm (Fig. 4*C*).

We next tested the Ca^{2+} fluorophore Fura-Red that can be excited using the visible light argon laser lines 458 and 488 nm (38). Unlike most other Ca^{2+} indicators, Fura-Red fluorescence *decreases* once the indicator binds Ca^{2+}. The emission ratio ($F_{458\ nm}/F_{488\ nm}$), however, increases with rising Ca^{2+} concentration (38). Fura-Red stained the parasite (Fig. 5*A*) and stable fluorescence intensities ($F_{458\ nm}$ and $F_{488\ nm}$) were recorded for both cytoplasm and food vacuole (Fig. 5*B*). The integrity of the food vacuole was not affected during the measurement, as verified using LS Blue (Fig. 5*B*). When the pH dependence of Fura-Red was investigated (see above), only minor effects were observed *in situ* (Fig. 6*A*). This finding was confirmed under *in vitro* cell-free conditions using a fluorospectrometer to scan the

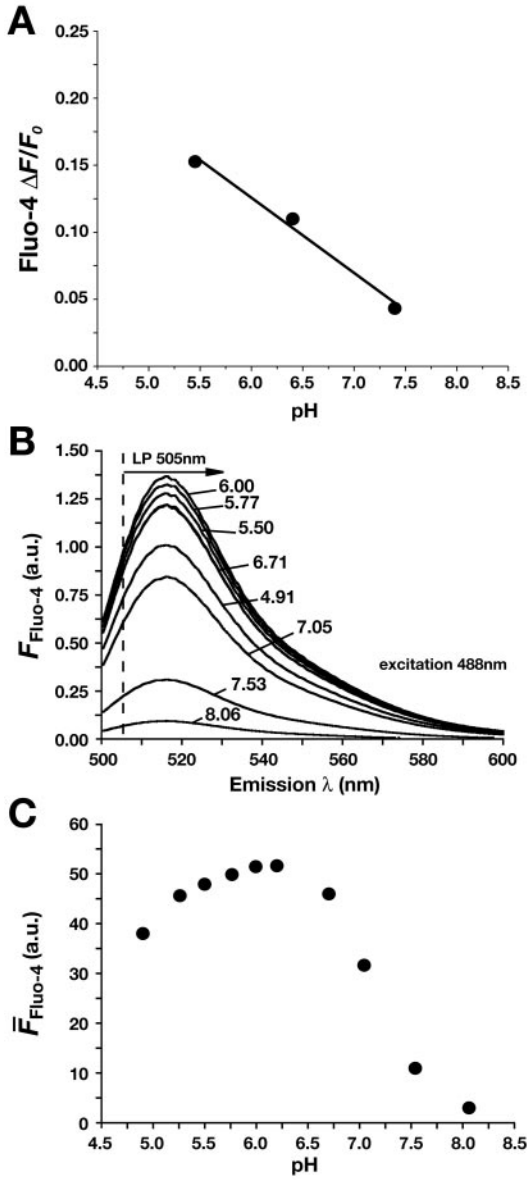

FIG. 3. **Fluo-4 fluorescence is pH-dependent.** *A*, the Fluo-4 fluorescence signal obtained from the *P. falciparum* food vacuole (*in situ*) was quantified from a recurrent illumination series and normalized to the initial value. The change in fluorescence ($\Delta F/F_0$) with varying pH is shown. The sizes of the error bars are smaller than the sizes of the circles and are, for this reason, not visible in the graph. *B*, *in vitro* Fluo-4 emission spectra recorded at a fixed free Ca^{2+} concentration of 350 nM and varying pH, as indicated. *C*, integrated fluorescence-pH relationship ($\bar{F}$) for a long pass filter (*LP*) of 505 nm, as used for the *in situ* experiments ($n > 5$). *a.u.*, arbitrary units.

emission spectra at both excitation wavelengths at different pH values ranging from 5.00 to 7.83 (Fig. 6*B*). A slight pH dependence of each excitation spectrum was observed. Importantly, the ratio of the 458 and 488 nm fluorescence intensities revealed almost no pH dependence, at least over the pH range tested (Fig. 6*C*).

Resting Subcellular $[Ca^{2+}]_i$—We next attempted steady-state Ca^{2+} measurements in different compartments of *P. falciparum*-infected erythrocytes using Fura-Red in a confocal setting. To convert confocally obtained $F_{458\ nm}/F_{488\ nm}$ ratios to free $[Ca^{2+}]_i$, we performed an *in situ* calibration by clamping the intracellular Ca^{2+} concentration of *P. falciparum*-infected erythrocytes to various free Ca^{2+} concentrations and measured the $F_{458\ nm}/F_{488\ nm}$ ratios in the food vacuole, the parasite cytoplasm, and the cytosol of the host erythrocyte (Fig. 7). This

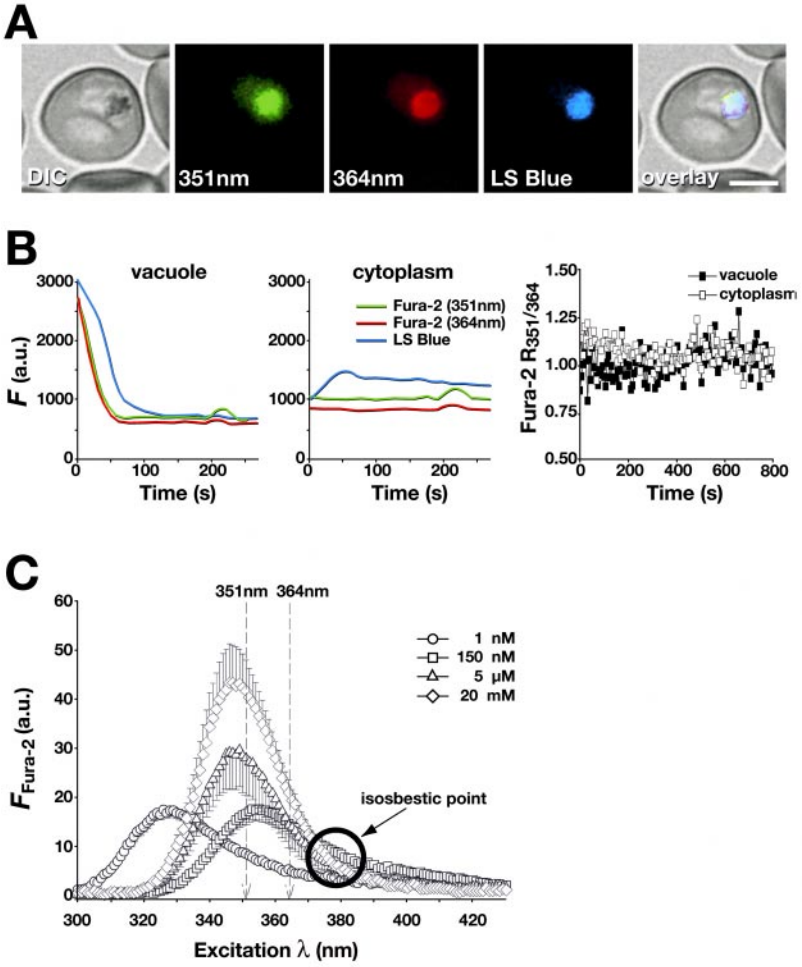

FIG. 4. **Live cell confocal and epifluorescent Fura-2 imaging of *P. falciparum*.** *A*, initial images from a recurrent illumination series of confocal Fura-2 recording (excited at 351 and 364 nm) obtained from a representative *P. falciparum*-infected erythrocyte co-stained with LS Blue. *Scale bar*, 5 μm. *B*, time course of Fura-2 and LS Blue fluorescence intensities recorded from the vacuole (*left*) and cytoplasm (*middle*). The *right panel* shows the time course of the ratio of the two Fura-2 fluorescence intensities ($F_{351\ nm}/F_{364\ nm}$) recorded from the food vacuole and the cytoplasm. Note: The ratios remain constant despite the redistribution of dye during the course of the experiment. *C*, Fura-2 spectra recorded from the cytoplasm of *P. falciparum*-infected erythrocytes in an epifluorescence setting. The Fura-2 spectra were recorded at different clamped intracellular Ca^{2+} concentrations, as indicated. The confocal laser lines (351 and 364 nm) are shown as *dashed lines*. The isosbestic point of Fura-2 in our specimen is indicated by a *circle*. The mean ± S.E. of six independent determinations are shown. *a.u.*, arbitrary units.

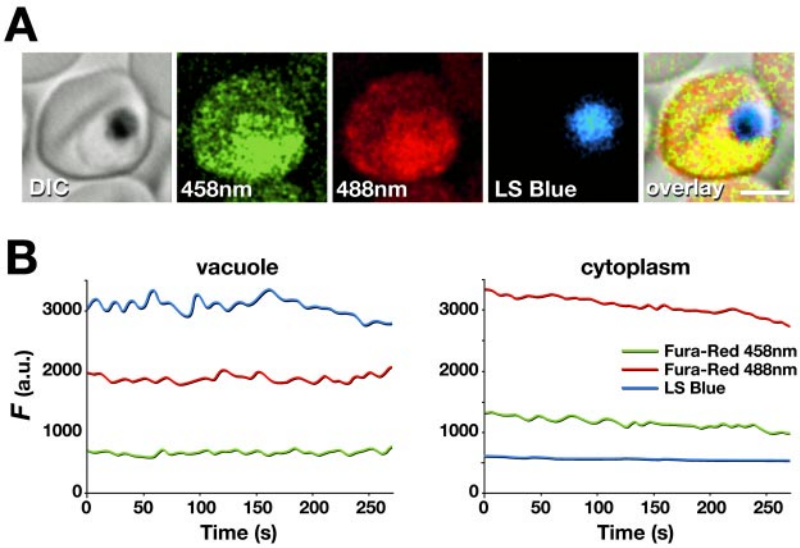

FIG. 5. **Confocal live cell Fura-Red imaging of *P. falciparum*-infected erythrocytes.** *A*, initial images from a recurrent illumination series of a confocal Fura-Red fluorescence recording (excited at 458 and 488 nm) obtained from a representative *P. falciparum*-infected erythrocyte co-stained with LS Blue. Note: Food vacuolar fluorescence intensity is decreased, implying higher free $[Ca^{2+}]_i$ as compared with the cytoplasm. *Scale bar*, 3 μm. *DIC*, differential interference contrast. *B*, the time course of the two fluorescence intensities of Fura-Red measured from the parasite's food vacuole and the cytoplasm. LS Blue fluorescence intensity is included to verify the intactness of the food vacuolar membrane. The time course remained stable throughout the illumination period. Note: LS Blue fluorescence was corrected for photobleaching, assuming a single exponential process with a decay time constant, determined by recurrent illumination under *in vitro* conditions. *a.u.*, arbitrary units.

approach allowed an independent calibration to be performed in each compartment separately. Possible contributions from autofluorescence or quenching were therefore taken into account. In addition, we measured uninfected erythrocytes and obtained a resting free $[Ca^{2+}]_i$ of 162 ± 18 nM (n = 54) (Table I), consistent with previous determinations (8, 9). In the cytosol of infected erythrocytes, the resting free $[Ca^{2+}]_i$ was significantly lower (86 ± 12 nM; n = 19; $p < 0.001$) (Table I). In the

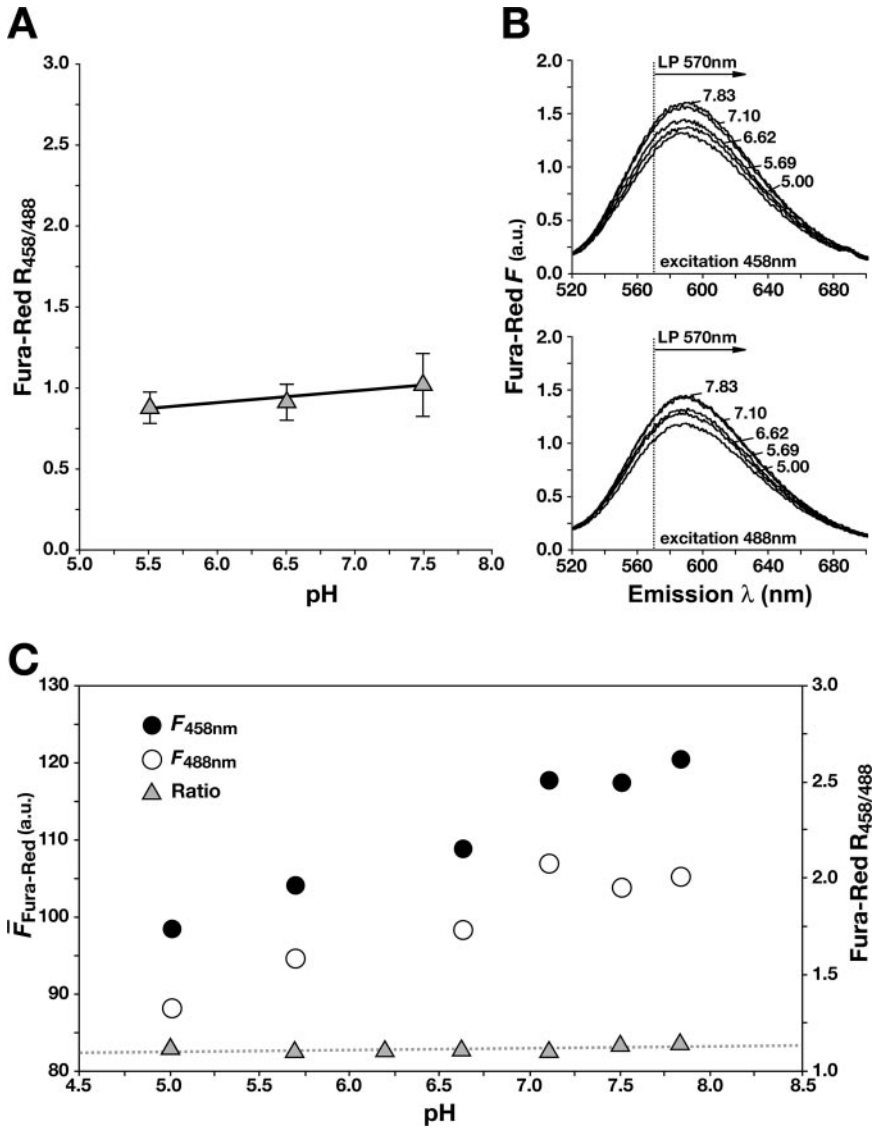

FIG. 6. **Fura-Red fluorescence and pH dependence.** *A*, *P. falciparum*-infected erythrocytes were stained with Fura-Red, and the food vacuolar fluorescence was quantified *in situ* at different pH values. The ratio ($R_{458/488}$) is shown as a function of the pH. *B*, *in vitro* emission spectra of Fura-Red excited either at 458 nm (*top*) or at 488 nm (*bottom*) in the presence of a fixed Ca^{2+} concentration of 350 nM and varying pH. *C*, integrated Fura-Red fluorescence ($\bar{F}$) for a long pass filter (*LP*) of 570 nm as used for the *in situ* measurements as a function of the pH. Note: The ratio ($R_{458/488}$) is largely pH independent, unlike the individual $F_{458\ nm}$ and $F_{488\ nm}$ fluorescence intensities. *a.u.*, arbitrary units.

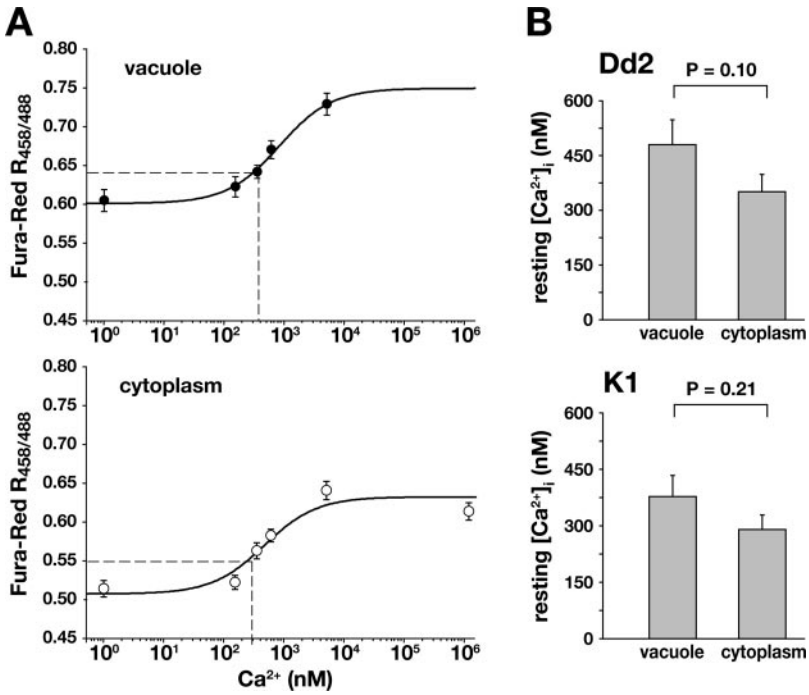

FIG. 7. ***In situ* calibration of Fura-Red fluorescence and determination of apparent resting free Ca^{2+} concentrations ($[Ca^{2+}]_i$) in the *P. falciparum* food vacuole and cytoplasm.** *A*, the Ca^{2+} equilibration curves for the steady-state Fura-Red fluorescence ratios ($F_{458\ nm}/F_{488\ nm}$) obtained from the food vacuole and cytoplasm of the *P. falciparum* clone K1 are shown. Cells were permeabilized with the Ca^{2+} ionophore ionomycin and adjusted to the Ca^{2+} concentrations indicated. The mean ± S.E. of 46 independent determinations is shown. The *solid lines* represent least square Hill fits to the data points (food vacuole, $r^2 = 0.99$; cytoplasm, $r^2 = 0.87$). *B*, evaluated mean apparent resting free Ca^{2+} concentrations ($[Ca^{2+}]_i$) determined for the *P. falciparum* clones K1 and Dd2. The numbers of indepen dent determinations are as follows: for K1, $n_{cyt} = 45$, and $n_{vac} = 46$; for Dd2, $n_{cyt} = 73$, and $n_{vac} = 55$.

TABLE I

Steady-state apparent free Ca^{2+} concentrations, $[Ca^{2+}]_i$, determined in the parasite's food vacuole, the cytoplasm and the host erythrocyte cytosol (infected red blood cells (iRBC))

The two different *P. falciparum* strains Dd2 and K1 were investigated. Uninfected erythrocytes (RBC) were examined in parallel. NA, not applicable.

	$[Ca^{2+}]_i$ vacuole	$[Ca^{2+}]_i$ cytoplasm
	nM ± S.E.	nM ± S.E.
Dd2	480 ± 64 (n = 55)[a,b]	352 ± 42 (n = 73)[b,c]
K1	375 ± 57 (n = 46)[a,d]	289 ± 39 (n = 45)[c,d]
iRBC	NA	86 ± 12 (n = 19)[e]
RBC	NA	162 ± 18 (n = 54)[a]

[a] $p = 0.22$.
[b] $p = 0.10$.
[c] $p = 0.27$.
[d] $p = 0.21$.
[e] $p = 0.0008$.

food vacuole of Dd2, we measured a resting free $[Ca^{2+}]_i$ value of 480 ± 64 nM (n = 55), and in the parasite's cytoplasm, we measured a resting free $[Ca^{2+}]_i$ value of 352 ± 42 nM (n = 73) (Table I). To compare these values, we repeated the determinations using a second strain. For K1, resting free $[Ca^{2+}]_i$ values of 375 ± 57 nM (n = 46) for the food vacuole and 289 ± 39 nM (n = 45) for the cytoplasm were obtained (Table I). The strain variations observed were not statistically significant ($p > 0.1$).

The cytoplasmic resting free $[Ca^{2+}]_i$ values determined in both strains are much higher than the cytosolic value of ~100 nM found in most eukaryotic cells under physiological conditions. This discrepancy led us to investigate to which extent the ER contributes to the measured cytoplasmic resting free $[Ca^{2+}]_i$. To determine the scope of the parasite's ER, we stained *P. falciparum*-infected erythrocytes with the fluorescent ER-Tracker Blue-White DPX dye. A confocal fluorescence signal was observed that occupied a large portion of the parasite's cytoplasm (Fig. 8), suggesting an extensive ER.

X-ray Microanalysis of P. falciparum—To localize possible Ca^{2+} stores within the parasite, total Ca^{2+} was assessed using x-ray microanalysis on unfixed entire *P. falciparum*-infected erythrocytes air-dried on Formvar/carbon-coated transmission electron microscopy grids. This is an established method to localize organelles with high ion content, including Ca^{2+} (41–44, 46–48). No Ca^{2+} hotspots were found (Fig. 9*A*). In comparison, x-ray microanalysis revealed a discrete hotspot for iron (Fig. 9*A*), which most likely co-localizes with the parasite's food vacuole, in which iron-containing heme accumulates and crystallizes to hemozoin. No iron hotspot was found in uninfected erythrocytes (Fig. 9*B*). X-ray spectra recorded from defined regions of interest, lying outside and within the iron-rich area detected in infected erythrocytes, confirmed that the iron does not coincide with a calcium hotspot (Fig. 10).

We repeated the study, under conditions of Ca^{2+} retention (41, 42), using 500-nm-thick cryofixed sections of *P. falciparum*-infected erythrocytes. As revealed by both elemental mapping and x-ray spectra recordings, the sections showed that the iron hotspot clearly coincides with the food vacuole (Fig. 11). Although this compartment is rich in iron, it does not appear to accumulate detectable levels of Ca^{2+} ($n > 10$) (Fig. 11). Interestingly, the food vacuole appears to have significantly less phosphorus than other subcellular compartments. For example, a high phosphorus and sulfur content was detected in small unidentified electron-dense organelles within the parasite (Fig. 11, *A* and *B*).

The Effect of TG and CPA on Ca^{2+} Dynamics—A previous study has suggested that a TG- and CPA-sensitive Ca^{2+}-ATPase is involved in maintaining Ca^{2+} homeostasis in the parasite's food vacuole (16). Using Fura-Red in a confocal setting, we investigated the effect of TG (1 μM) and CPA (10 μM) on subcellular Ca^{2+} dynamics. In the case of CPA, a slight increase in free $[Ca^{2+}]_i$ was observed in the parasite's food vacuole and cytoplasm and in the cytosol of the host erythrocyte (Fig. 12). For TG, even less pronounced effects on Ca^{2+} dynamics were detected (Fig. 12).

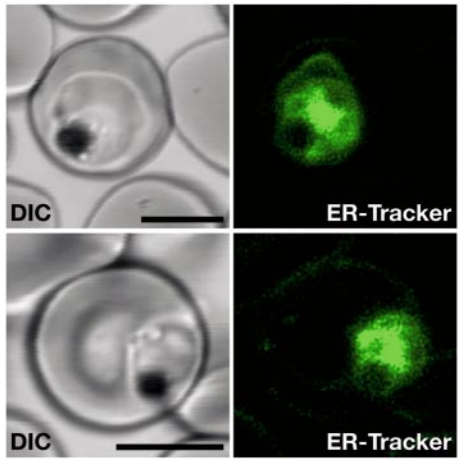

FIG. 8. **Confocal live cell imaging of *P. falciparum*-infected erythrocytes using the ER-Tracker Blue-White DPX.** The ER staining is seen throughout the whole cytoplasm, whereas the food vacuole region remains unstained. These are two representative images of n = 10 tested parasites. *Scale bar*, 5 μm. *DIC*, differential interference contrast.

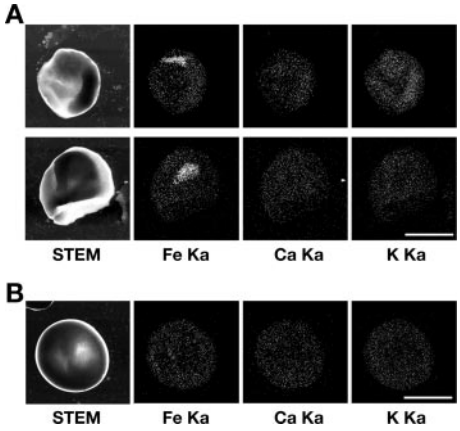

FIG. 9. **Scanning transmission electron micrographs (*STEM*) and elemental mapping of infected (*A*) and uninfected (*B*) erythrocytes.** Whole cells were spotted and air-dried onto the EM grids, and the ions iron (*Fe*), Ca^{2+} (*Ca*), and potassium (*K*) were mapped. *Scale bar*, 4 μm. *Ka*, K_α energetic state of the respective ion.

DISCUSSION

Studies on steady-state and dynamic Ca^{2+} in *P. falciparum*-infected erythrocytes have been complicated by the small size of the specimen, the numerous subcellular compartments, and the resulting difficulties in the spatial resolution. We have evaluated different fluorimetric Ca^{2+} indicators in a confocal setting and found that, for *P. falciparum*-infected erythrocytes, Fura-Red has several advantages over other Ca^{2+}-sensitive fluorochromes in resolving free $[Ca^{2+}]_i$ in different subcellular compartments, including the parasite's acidic food vacuole. Fura-Red supports ratiometric Ca^{2+} recordings in a confocal arrangement (38). Its favorable excitation (458 and 488 nm) and emission wavelengths (maximum ~590 nm) minimize interference from human erythrocyte autofluorescence (~520–560 nm, data not shown). The fluorescence signal ratio is largely pH independent, at least within the physiological pH

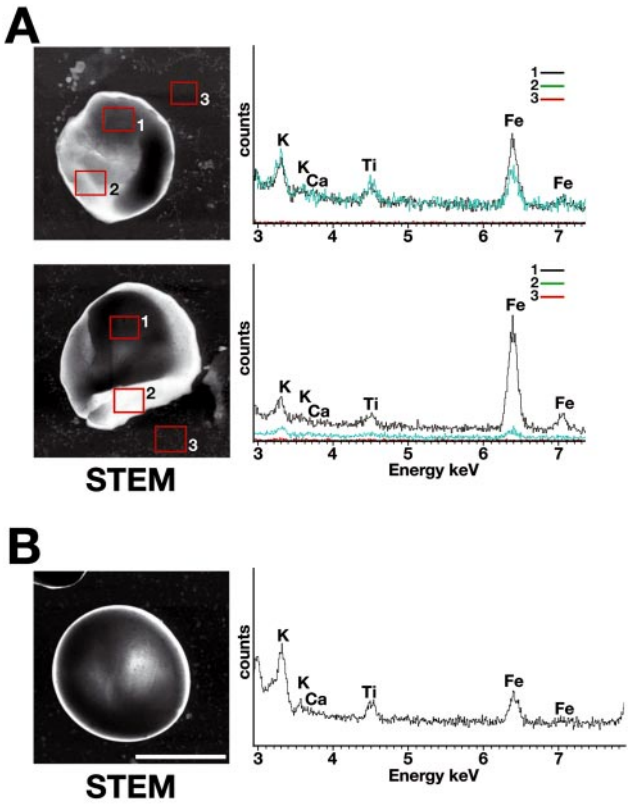

FIG. 10. **X-ray spectral analysis of uninfected and *P. falciparum*-infected erythrocytes.** *A*, the same *P. falciparum*-infected erythrocytes as shown in Fig. 9 were used to measure ion compositions in various regions of interest. Iron can be seen mainly in one region. There is no detectable Ca^{2+} peak. The two potassium and iron peaks shown in the spectra correspond to the K_α and K_β energetic states of the respective ion. Titanium comes from the specimen holder. The background (region 3) indicated in *red* lies close to the *x* axis. *B*, uninfected erythrocyte. *Scale bar*, 4 μm.

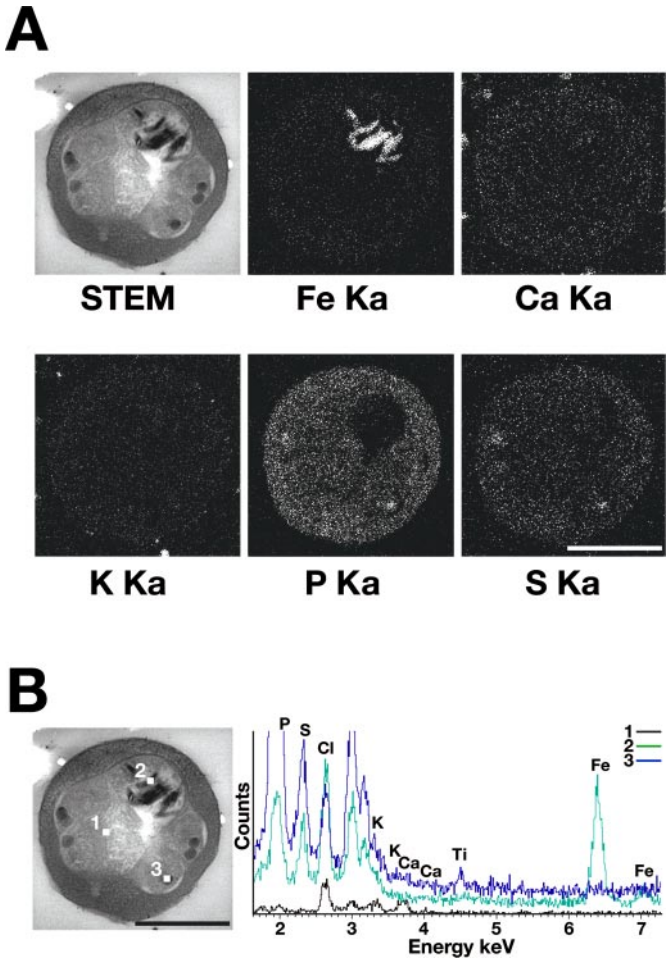

FIG. 11. **Cryosection of a *P. falciparum*-infected erythrocyte.** *A*, elemental mapping of a 500-nm-thick cryosection of a *P. falciparum*-infected erythrocyte. The iron hotspot correlates with the food vacuole. Ca^{2+} (*Ca*) and potassium (*K*) are evenly distributed throughout the parasite. Note the reduced phosphorus (*P*) counts from the parasite's food vacuole and the two phosphorus- and sulfur- (*S*) rich unidentified electron-dense compartments. *B*, x-ray spectra of the cryosection. Regions of interest were selected to measure the abundance of the various elements selected. *Scale bar*, 3 μm. *Ka*, K_α, energetic state of the respective ion.

range tested (Fig. 6), and Fura-Red does not appear to photosensitize the specimen, allowing stable time-lapse recordings to be made. This is a major advantage, as photolysis of the parasite's food vacuole arises quickly during live cell imaging of *P. falciparum*-infected erythrocytes due to light-induced lipid peroxidation (34). In the case of Fura-Red, photolysis was not a concern, as verified using the acidotropic fluorochrome LS Blue as an indicator for food vacuolar integrity (34).

In comparison with Fura-Red, Fluo-4 appears to be less advantageous for *P. falciparum*-infected erythrocytes, although it has been used in previous studies (16). Fluo-4 lacks a clear isosbestic point, precluding its use in ratiometric measurements. Therefore, Fluo-4 fluorescence signals are dependent on dye loading and partitioning. Moreover, Fluo-4 fluorescence is pH-dependent. Interestingly, its pH dependence is reversed as compared with that of the related fluorochromes, Fluo-3 and fluorescein (33, 49, 50). In the case of Fluo-4, the fluorescence intensity increases as the pH decreases (Fig. 3). The implications on live cell Ca^{2+} imaging of *P. falciparum* are discussed below.

Fluo-4 appears to aggravate the photosensitivity of the specimen. During the course of this study, we repeatedly noticed the light sensitivity of the preparation and how quickly the parasite's food vacuole lyses during Fluo-4 fluorescence imaging, as compared with Fura-Red using the same experimental conditions (Figs. 1 and 2). The decrease in fluorescence of both Fluo-4 and LS Blue in the food vacuole and the concomitant increase in the cytoplasm are consistent with photo-induced damage to the food vacuolar membrane (34). Leakage of this compartment may result in a redistribution of the dyes from the food vacuole into the cytoplasm and/or a discharge of the food vacuolar acid load. Because of the intrinsic pH dependence of Fluo-4, a collapse of the pH gradient across the food vacuolar membrane will have a profound effect on Fluo-4 fluorescence signals. We acknowledge that photo damage is cumulative and may increase with the number of fluorochromes investigated simultaneously (Figs. 1 and 2, compare Fluo-4 labeling alone with that of Fluo-4 and LS Blue).

We further tested Fura-2, which is a UV light-excitable ratiometric Ca^{2+} indicator that has been mainly used for wide field fluorescence microscopy (15, 51). Its chemical structure differs from that of Fluo-4. Photo-bleaching is eliminated due to the ratiometric nature of the dye. In *P. falciparum*-infected erythrocytes stained with Fura-2, we observed a red shift of the isosbestic point, preventing its use as a ratiometric dye in a confocal setting with 351- and 364-nm laser lines.

Using Fluo-4, a previous study has argued that the parasite's acidic food vacuole is a dynamic intracellular Ca^{2+} store (16). This conclusion was based on the preferential Fluo-4 staining of the food vacuole in the strain investigated (16) (see also Fig. 2). From the Fluo-4 image, the apparent free Ca^{2+} concentration of the food vacuole was calculated to be 5-fold higher than

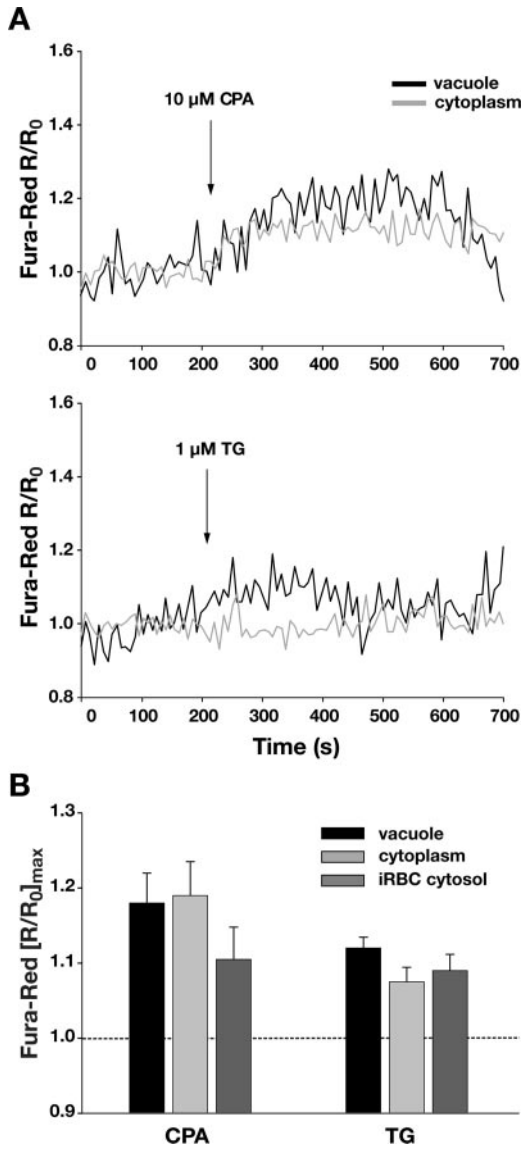

FIG. 12. **Food vacuolar and cytoplasmic dynamics of Fura-Red Ca^{2+} fluorescence in *P. falciparum* in the presence of the Ca^{2+} modulators CPA and TG.** *A*, the time course of food vacuolar and cytoplasmic Fura-Red Ca^{2+} fluorescence intensity ratios ($r = F_{458\ nm}/F_{488\ nm}$) relative to their value before application of either 10 μM CPA (*top*) or 1 μM TG (*bottom*) (R_0). R/R_0 is shown in two representative parasites. An increase in Ca^{2+} fluorescence can be observed, which is more pronounced for CPA. *B*, summary of the maximum drug-induced changes $[R/R_0]_{max}$ in the parasite's food vacuole and cytoplasm, as well as in the host erythrocyte (infected red blood cells (*iRBC*)) cytosol. The mean ± S.E. of least five independent determinations are shown (*dashed line*, reference before drug application).

in the cytosol (16). It was further suggested, again based on Fluo-4 imaging, that the food vacuolar free $[Ca^{2+}]_i$ is maintained by a TG- and CPA-sensitive Ca^{2+}-ATPase (16).

Our data agreed with these observations only to some extent. Using Fura-Red, we observed, in the presence of CPA, a slight increase in free $[Ca^{2+}]_i$ in the food vacuole but no decline as predicted by Biagini *et al.* (16). Moreover, a slight increase in free $[Ca^{2+}]_i$ was observed in the parasite's cytoplasm and in the host erythrocyte cytosol upon the addition of CPA. TG had even less of an effect on Ca^{2+} dynamics. Our findings were more consistent with an inhibition of an endoplasmic Ca^{2+}-ATPase by CPA and a subsequent redistribution of Ca^{2+} from the ER into other subcellular compartments as opposed to the inhibition of a food vacuolar Ca^{2+}-ATPase. In accordance with our conclusion, previous studies have noted a discharge of Ca^{2+} from the ER, but not from the food vacuole, in the presence of CPA (15, 19). For TG, only a slight, if any, effect on Ca^{2+} dynamics in *P. falciparum* was reported (15, 19), again consistent with our data. The redistribution of Fluo-4 fluorescence signal from the food vacuole to the cytoplasm was typically observed after photolysis of the parasite's food vacuolar membrane (Fig. 1).

When measuring steady-state Ca^{2+} using Fura-Red, we observed an apparent resting free $[Ca^{2+}]_i$ in the food vacuole of 370–480 nM, depending on the strain investigated. Importantly, we found that the food vacuolar free $[Ca^{2+}]_i$ is slightly albeit not significantly higher as compared with the cytoplasm, for which we obtained values ranging from 289 to 352 nM, depending on the strain investigated. The cytoplasmic values are unexpectedly high given that free $[Ca^{2+}]_i$ in the cytosol of eukaryotic cells is usually in the order of 100 nM (14). However, we do not believe that our determinations are compromised. A previous study has reported similar cytoplasmic values for *P. falciparum*, as determined by measuring populations of parasites isolated from their host cell and stained with Fura-2, in a spectral-fluorimetric setting (15).

Further validation of our experimental approach comes from Ca^{2+} measurements within uninfected erythrocytes. Simultaneous recordings of the apparent free $[Ca^{2+}]_i$ in the cytosol of uninfected erythrocytes (only a small number of erythrocytes are infected in the preparation) provided values comparable with previous determinations (Table I) (13, 15). For the cytosol of infected erythrocytes, we obtained values that were even lower than those found for uninfected erythrocytes (Table I), which may suggest that the parasite exploits its host cell regarding free Ca^{2+}.

Then how can the high apparent resting $[Ca^{2+}]_i$ measured in the parasite's cytoplasm be explained? *P. falciparum* replicates within 48 h, releasing 8–32 daughter cells. We reasoned that this replication rate necessitates a high rate of protein synthesis, which in turn requires an extensive ER. Using an established ER tracker, we indeed found that the ER of the parasite occupies a large portion of the cytoplasmic region (Fig. 8). On the basis of these considerations, we favor the hypothesis that the high apparent resting free $[Ca^{2+}]_i$ measured in the parasite's cytoplasm is a superposition of Ca^{2+} concentrations from both the cytosol and the ER. The large extension of the ER and the contribution of the ER to fluorimetric Ca^{2+} determinations may have been underestimated in previous studies.

Since the cytoplasmic and food vacuolar apparent free $[Ca^{2+}]_i$ are so similar, the difference in the Fluo-4 fluorescence signals from these two compartments must be due to another factor. Indeed, there exists a large pH gradient across the parasite's food vacuolar membrane, from 7.3 in the cytoplasm (36) to ~5.4 in the food vacuole (30). The pH dependence of the Fluo-4 fluorescence signal, together with the vastly different standing pH values in cytoplasm and food vacuole, may explain why fluorescence intensities measured from these two compartments are different despite their similar resting free $[Ca^{2+}]_i$.

The apparent free $[Ca^{2+}]_i$ of ~400 nM measured in the food vacuole indicates a low amount of exchangeable Ca^{2+}. This, however, does not necessarily contradict a function as a Ca^{2+} store. As shown for the plant tonoplast, the yeast vacuole and the acidocalcisomes of different protozoa, most of the millimolar to molar amount of Ca^{2+} is complexed with polyphosphate in a relatively stable form and is therefore non-exchangeable (24, 32, 52, 53). In the case of the *P. falciparum* food vacuole, however, neither elemental mapping nor x-ray spectra recordings provided evidence for high concentrations of total calcium or even phosphorus. The x-ray microanalysis was designed to

retain Ca^{2+}. According to previous experience with this technology, compartmentalized enrichment of Ca^{2+} should be detectable, with threshold Ca^{2+} levels slightly above basal cytosolic Ca^{2+} values (43, 44, 47, 48). Consistent with our data, another study also found no indication of a high phosphorus concentration in the *P. falciparum* food vacuole (54). On the basis of these considerations, we propose that the *P. falciparum* food vacuole plays only a minor role, if any, in Ca^{2+} storage.

Acknowledgments—We thank Kathrin Steigleder and Elisabeth Wilken for technical assistance.

REFERENCES

1. World Health Organization (2000) *World Health Organ. Tech. Rep. Ser.* **892,** i–v, 1–74
2. Billker, O., Dechamps, S., Tewari, R., Wenig, G., Franke-Fayard, B., and Brinkmann, V. (2004) *Cell* **117,** 503–514
3. Garcia, C. R. (1999) *Parasitol. Today* **15,** 488–491
4. Eckstein-Ludwig, U., Webb, R. J., Van Goethem, I. D., East, J. M., Lee, A. G., Kimura, M., O'Neill, P. M., Bray, P. G., Ward, S. A., and Krishna, S. (2003) *Nature* **424,** 957–961
5. Caldas, M. L., and Wasserman, M. (2001) *Int. J. Parasitol.* **31,** 776–782
6. Krishna, S., Woodrow, C., Webb, R., Penny, J., Takeyasu, K., Kimura, M., and East, J. M. (2001) *J. Biol. Chem.* **276,** 10782–10787
7. Tanabe, K. (1990) *Blood Cells* **16,** 437–449
8. Engelmann, B. (1991) *Klin. Wochenschr.* **69,** 137–142
9. Harrison, D. G., and Long, C. (1968) *J. Physiol.* (*Lond.*) **199,** 367–381
10. Tanabe, K., Mikkelsen, R. B., and Wallach, D. F. (1982) *J. Cell Biol.* **93,** 680–684
11. Desai, S. A., McCleskey, E. W., Schlesinger, P. H., and Krogstad, D. J. (1996) *Am. J. Trop. Med. Hyg.* **54,** 464–470
12. Sherman, I. W. (1985) *Parasitology* **91,** 609–645
13. Camacho, P. (2003) *J. Cell Biol.* **161,** 17–19
14. Berridge, M. J., Bootman, M. D., and Roderick, H. L. (2003) *Nat. Rev. Mol. Cell. Biol.* **4,** 517–529
15. Alleva, L. M., and Kirk, K. (2001) *Mol. Biochem. Parasitol.* **117,** 121–128
16. Biagini, G. A., Bray, P. G., Spiller, D. G., White, M. R., and Ward, S. A. (2003) *J. Biol. Chem.* **278,** 27910–27915
17. Gazarini, M. L., Thomas, A. P., Pozzan, T., and Garcia, C. R. (2003) *J. Cell Biol.* **161,** 103–110
18. Garcia, C. R., Ann, S. E., Tavares, E. S., Dluzewski, A. R., Mason, W. T., and Paiva, F. B. (1998) *Eur. J. Cell Biol.* **76,** 133–138
19. Varotti, F. P., Beraldo, F. H., Gazarini, M. L., and Garcia, C. R. (2003) *Cell Calcium* **33,** 137–144
20. Garcia, C. R., Dluzewski, A. R., Catalani, L. H., Burting, R., Hoyland, J., and Mason, W. T. (1996) *Eur. J. Cell Biol.* **71,** 409–413
21. Marchesini, N., Luo, S., Rodrigues, C. O., Moreno, S. N., and Docampo, R. (2000) *Biochem. J.* **347,** 243–253
22. Moreno, S. N., and Docampo, R. (2003) *Curr. Opin. Microbiol.* **6,** 359–364
23. Docampo, R., de Souza, W., Miranda, K., Rohloff, P., and Moreno, S. N. (2005) *Nat. Rev. Microbiol.* **3,** 251–261
24. Docampo, R., and Moreno, S. N. (1999) *Parasitol. Today* **15,** 443–448
25. Docampo, R., and Moreno, S. N. (2001) *Mol. Biochem. Parasitol.* **114,** 151–159
26. Ruiz, F. A., Luo, S., Moreno, S. N., and Docampo, R. (2004) *Microsc. Microanal.* **10,** 563–567
27. Goldberg, D. E., Slater, A. F., Cerami, A., and Henderson, G. B. (1990) *Proc. Natl. Acad. Sci. U. S. A.* **87,** 2931–2935
28. Sullivan, D. J., Jr., Gluzman, I. Y., and Goldberg, D. E. (1996) *Science* **271,** 219–222
29. Olliaro, P. L., and Goldberg, D. E. (1995) *Parasitol. Today* **11,** 294–297
30. Bennett, T. N., Kosar, A. D., Ursos, L. M., Dzekunov, S., Singh Sidhu, A. B., Fidock, D. A., and Roepe, P. D. (2004) *Mol. Biochem. Parasitol.* **133,** 99–114
31. Halachmi, D., and Eilam, Y. (1989) *FEBS Lett.* **256,** 55–61
32. Dunn, T., Gable, K., and Beeler, T. (1994) *J. Biol. Chem.* **269,** 7273–7278
33. Haugland, R. P. (2002) *Handbook of Fluorescent Probes and Research Products*, Ninth Ed., Molecular Probes, Inc., Eugene, OR
34. Wissing, F., Sanchez, C. P., Rohrbach, P., Ricken, S., and Lanzer, M. (2002) *J. Biol. Chem.* **277,** 37747–37755
35. Trager, W., and Jensen, J. B. (1976) *Science* **193,** 673–675
36. Wunsch, S., Sanchez, C., Gekle, M., Kersting, U., Fischer, K., Horrocks, P., and Lanzer, M. (1997) *Behring Inst. Mitt.* **199,** 44–50
37. Wunsch, S., Sanchez, C. P., Gekle, M., Grosse-Wortmann, L., Wiesner, J., and Lanzer, M. (1998) *J. Cell Biol.* **140,** 335–345
38. Lohr, C. (2003) *Cell Calcium* **34,** 295–303
39. Friedrich, O., Both, M., Gillis, J. M., Chamberlain, J. S., and Fink, R. H. (2004) *J. Physiol.* (*Lond.*) **555,** 251–265
40. Knoll, G., Braun, C., and Plattner, H. (1991) *J. Cell Biol.* **113,** 1295–1304
41. Knoll, G., Grassle, A., Braun, C., Probst, W., Hohne-Zell, B., and Plattner, H. (1993) *Cell Calcium* **14,** 173–183
42. Poenie, M., and Epel, D. (1987) *J. Histochem. Cytochem.* **35,** 939–956
43. Hardt, M., and Plattner, H. (1999) *J. Struct. Biol.* **128,** 187–199
44. Hardt, M., and Plattner, H. (2000) *Eur. J. Cell Biol.* **79,** 642–652
45. Takahashi, A., Camacho, P., Lechleiter, J. D., and Herman, B. (1999) *Physiol. Rev.* **79,** 1089–1125
46. Miranda, K., Docampo, R., Grillo, O., and de Souza, W. (2004) *Protist* **155,** 395–405
47. Miranda, K., Docampo, R., Grillo, O., Franzen, A., Attias, M., Vercesi, A., Plattner, H., Hentschel, J., and de Souza, W. (2004) *Histochem. Cell Biol.* **121,** 407–418
48. Miranda, K., Rodrigues, C. O., Hentchel, J., Vercesi, A., Plattner, H., de Souza, W., and Docampo, R. (2004) *Microsc. Microanal.* **10,** 647–655
49. Lattanzio, F. A., Jr. (1990) *Biochem. Biophys. Res. Commun.* **171,** 102–108
50. Lattanzio, F. A., Jr., and Bartschat, D. K. (1991) *Biochem. Biophys. Res. Commun.* **177,** 184–191
51. Grynkiewicz, G., Poenie, M., and Tsien, R. Y. (1985) *J. Biol. Chem.* **260,** 3440–3450
52. Roos, W. (2000) *Planta* **210,** 347–370
53. Scott, D. A., Docampo, R., Dvorak, J. A., Shi, S., and Leapman, R. D. (1997) *J. Biol. Chem.* **272,** 28020–28029
54. Lee, P., Ye, Z., Van Dyke, K., and Kirk, R. G. (1988) *Am. J. Trop. Med. Hyg.* **39,** 157–165